THE ASTRONOMICAL JOURNAL, 121:267–282, 2001 January

HUBBLE SPACE TELESCOPE STIS OBSERVATIONS OF THE WOLF-RAYET STAR HD 5980 IN THE SMALL MAGELLANIC CLOUD. II. THE INTERSTELLAR MEDIUM COMPONENTS[1]

GLORIA KOENIGSBERGER, LEONID GEORGIEV, AND MANUEL PEIMBERT
Instituto de Astronomía, Universidad Nacional Autónoma de México, Apdo. Postal 70-264, 04510 México D.F., Mexico
NOLAN R. WALBORN
Space Telescope Science Institute, 3700 San Martin Drive, Baltimore, MD 21218
RODOLFO BARBÁ,[2] VIRPI S. NIEMELA,[3] AND NIDIA MORRELL[2]
Facultad de Ciencias Astronómicas y Geofísicas, Universidad Nacional de la Plata, Paseo del Bosque S/N, B19000FWA La Plata, Argentina
ZLATAN TSVETANOV
Department of Physics and Astronomy, Johns Hopkins University, 3400 North Charles Street, Baltimore, MD 21218-2686
AND
REGINA SCHULTE-LADBECK
Department of Physics and Astronomy, University of Pittsburgh, 3941 O'Hara Street, Pittsburgh, PA 15260
Received 2000 August 30; accepted 2000 October 2

ABSTRACT

Observations of the interstellar and circumstellar absorption components obtained with the *Hubble Space Telescope* Space Telescope Imaging Spectrograph (STIS) along the line of sight toward the Wolf-Rayet–luminous blue variable (LBV) system HD 5980 in the Small Magellanic Cloud are analyzed. Velocity components from C I, C I*, C II, C II*, C IV, N I, N V, O I, Mg II, Al II, Si II, Si II*, Si III, Si IV, S II, S III, Fe II, Ni II, Be I, Cl I, and CO are identified, and column densities estimated. The principal velocity systems in our data are (1) interstellar medium (ISM) components in the Galactic disk and halo ($V_{\rm hel} = 1.1 \pm 3$, 9 ± 2 km s^{-1}); (2) ISM components in the SMC ($V_{\rm hel} = +87 \pm 6$, $+110 \pm 6$, $+132 \pm 6$, $+158 \pm 8$, $+203 \pm 15$ km s^{-1}); (3) SMC supernova remnant SNR 0057−7226 components ($V_{\rm hel} = +312 \pm 3$, $+343 \pm 3$, $+33$, $+64$ km s^{-1}); (4) circumstellar (CS) velocity systems ($V_{\rm hel} = -1020$, -840, -630, -530, -300 km s^{-1}); and (5) a possible system at -53 ± 5 km s^{-1} (seen only in some of the Si II lines and marginally in Fe II) of uncertain origin. The supernova remnant SNR 0057−7226 has a systemic velocity of $+188$ km s^{-1}, suggesting that its progenitor was a member of the NGC 346 cluster. Our data allow estimates to be made of $T_e \sim 40{,}000$ K, $n_e \sim 100$ cm^{-3}, $N({\rm H}) \sim (4\text{–}12) \times 10^{18}$ cm^{-2} and a total mass between 400 and 1000 $M_\odot$ for the supernova remnant (SNR) shell. We detect C I absorption lines primarily in the $+132$ and $+158$ km s^{-1} SMC velocity systems. As a result of the LBV-type eruptions in HD 5980, a fast-wind/slow-wind circumstellar interaction region has appeared, constituting the earliest formation stages of a windblown H II bubble surrounding this system. Variations over a timescale of 1 year in this circumstellar structure are detected.

Key words: ISM: bubbles — stars: individual (HD 5980) — stars: winds, outflows — supernova remnants

1. INTRODUCTION

The Wolf-Rayet (W-R) binary system HD 5980 is the visually brightest stellar object in the Small Magellanic Cloud. It lies on the periphery of the largest SMC H II region, NGC 346, and it consists of a close ($P = 19.266$ days) eclipsing W-R binary system and a third component, which may itself be multiple (Koenigsberger et al. 2000). HD 5980 underwent two luminous blue variable–like eruptive events in 1993 and 1994, during which the wind velocities decreased and the mass-loss rates increased (Koenigsberger et al. 1998a, 1998b). During the eruptive phases, the wind velocities were $\sim$200–400 km s^{-1}, while during the subsequent "quiescent" phases of the system, wind velocities as fast as 3000 km s^{-1} prevailed. Hence, as the fast wind collides with the slower moving material ejected at the time of the eruption, gas is shocked, leading eventually to the formation of an H II region surrounding the system. Such a scenario is believed to apply to the Homunculus in η Carinae (Frank, Balick, & Davidson 1995; García-Segura, Mac Low, & Langer 1996), which is the result of the "Great Eruption" in 1850 (Morse, Humphreys, & Damineli 1999).

The current mass of the erupting star (called star A) in HD 5980 is estimated at $\sim 50\ M_\odot$, and that of the close companion (star B) at $\sim 28\ M_\odot$ (Niemela et al. 1997). However, when placed on an H-R diagram, with values $L_A = 3 \times 10^6\ L_\odot$ (Koenigsberger et al. 1998b) and $T_{\rm eff} = 21{,}000$ K (Koenigsberger et al. 1996) obtained for star A near the time of the 1994 eruption, it lies above the evolutionary tracks of a zero-age main-sequence star of 140 $M_\odot$, and to the right of the Humphreys-Davidson limit (Humphreys & Davidson 1979). Thus, assuming evolution in this binary system has proceeded according to the standard binary evolutionary scenarios, star A must have already lost over 90 $M_\odot$. Furthermore, star B is believed to

[1] Based on observations with the NASA/ESA *Hubble Space Telescope*, obtained at the Space Telescope Science Institute, which is operated by the Association of Universities for Research in Astronomy, Inc., under NASA contract NAS 5-26555.
[2] Member of Carrera del Investigador, CONICET, Argentina.
[3] Member of Carrera del Investigador, CIC, Prov. Buenos Aires, Argentina.

be a W-R star, implying that it, too, must have lost a significant amount of mass. Thus, the interstellar medium (ISM) surrounding HD 5980 may contain as much as 200 $M_{\odot}$ lost from this stellar system. HD 5980 is also a significant source of ionizing photons. Although near the maximum of the eruption the effective temperature of star A was relatively low, its "quiescent" temperature is over 50,000 K (Koenigsberger et al. 1998a; Schweickhardt & Schmutz 1999).

The two major eruptions that have occurred in HD 5980 within the past 7 years should have produced an ISM structure surrounding the system. Indeed, *Hubble Space Telescope* (*HST*) observations of HD 5980 carried out in 1999 revealed the presence of strong circumstellar absorption lines in C IV and Si IV, which most likely are related to the fast-wind/slow-wind interaction region resulting from the 1994 eruption. These absorption lines are found at velocities of ~ -680 km s^{-1} ($V_{\rm hel} \sim -530$ km s^{-1}) with respect to the SMC velocity (Koenigsberger et al. 2000). In this paper we search for additional such features, which should allow an analysis of the interacting winds.

HD 5980 is embedded in the N66 H II complex. This giant H II region has been observed at wavelengths ranging from radio to X-rays, and at least five distinct regions can be identified and were described by Ye, Turtle, & Kennicutt (1991). Two of these five regions are located along the line of sight to HD 5980. The first one consists of two nearly concentric shells present in Hα data, with their centers close to HD 5980 and diameters of 1.2 and 5.5, respectively. Based on identical images in Hα and [O III] (Czyzak & Aller 1977) and no enhancement of [S II] in the filamentary structure, Walborn (1978) suggested that the shell structure is a consequence of mass loss from HD 5980 and the nearby O7 supergiant Sk 80. The radio observations of Ye et al. (1991) confirmed the thermal nature of this component. The second component is a supernova remnant identified by Ye et al. (1991), who find a nonthermal shell radio source along the line of sight to HD 5980 having a diameter of 3.2 (55 pc) and close to which lies the X-ray source IKT 18 (Inoue, Koyama, & Tanaka 1983). Fitzpatrick & Savage (1983) had already suggested the presence of an SNR moving toward HD 5980 with a velocity of 150 km s^{-1} ($V_{\rm LSR} = 300$ km s^{-1}) based on *International Ultraviolet Explorer* (*IUE*) data, in which ISM absorption features shifted by this velocity were detected (de Boer & Savage 1980). Chu & Kennicutt (1988) also detected the presence of clumps moving at up to ~ 170 km s^{-1} with respect to the H II region in their Hα and [N II] echelle observations with the slit placed at the position of the nonthermal source. This SNR (SNR 0057$-$7226) is the second most luminous SNR in the SMC at 843 MHz.

In addition to the velocity system associated with the SNR, de Boer & Savage (1980) used *IUE* observations along the line of sight to HD 5980 in order to identify absorption line systems at $V_{\rm hel}$ in the range 80–220 km s^{-1}. These velocities were shown to correspond to the SMC H II regions from optical Ca II observations by Songaila et al. (1986), who concluded that the SMC appears to consist of layers of ISM gas at different velocities and distances. More recently, Welty et al. (1997) have used Goddard High Resolution Spectrograph observations along the line of sight to the SMC star Sk 108 and have determined the presence of at least 16 individual cloud velocity systems between 80 and 210 km s^{-1} and nine individual cloud systems at Galactic velocities. They obtain relative gas-phase abundances for the SMC lines of Si II, Cr II, Mn II, Fe II, Ni II, and Zn II that are similar to those found for ISM clouds in the Galactic halo. A similar study along the line of sight to HD 5980 would be most desirable, although the degree of contamination by the SNR and by possible shells ejected from HD 5980 in previous eruptive phases needs first to be analyzed.

This paper is organized as follows: § 2 contains the description of the data; in § 3, we determine the general velocity systems that are present in these *HST* data; in § 4, we present estimates of the column densities derived for all the observed ISM-like features in the spectrum; and in § 5 we present the summary and conclusions.

2. OBSERVATIONS AND DATA ANALYSIS

As part of *HST* Cycle 7 General Observer program 7480, six high-resolution spectra of HD 5980 were obtained with the Space Telescope Imaging Spectrograph (STIS; Woodgate et al. 1998), five during 1999 May and one in 2000 April. The MAMA detector was used with the E140M grating, obtaining a resolution of ~ 4 km s^{-1} in the 1150–1710 Å wavelength range. Further details may be found in Koenigsberger et al. (2000). The spectra were processed through the standard STScI pipeline. The signal-to-noise ratio (S/N) of each individual spectrum is ~ 40, at 1400 Å. Averaging the five spectra obtained in 1999 gives an enhanced S/N ~ 70. This average, flux-calibrated spectrum was used to search for all lines arising from ground-state transitions with wavelengths in the range 1150–1700 Å, using the tables of line identifications of Kelly & Palumbo (1973) and the electronically available line lists at the National Institute of Standards and Technology (NIST).

The data were analyzed using IRAF[4] routines to measure wavelength positions and the equivalent widths. Gaussian functions were generally employed to fit the line profiles to perform the measurements. When necessary, absorptions were fitted with several (two to four) Gaussians, which allows the lines to be deblended and principal velocities and equivalent widths to be assigned to individual components of a blend. No attempt was made, however, to perform a fit for the large number (nine Galactic and 16 in the SMC; Welty et al. 1997) of individual velocity components contributing to the absorptions. In the cases where one or several Gaussians provided a poor fit, the equivalent width was obtained by directly integrating the flux over the specified wavelength range.

One of the major sources of uncertainty in the equivalent width measurements is the placement of the continuum level. The spectrum of HD 5980 contains broad emission and P Cygni lines originating in the stellar winds, as well as weak photospheric absorption components, and many of the ISM components are superposed upon these features. Thus, in many cases, the local "continuum" level corresponds to the flux level of the P Cygni emission line, at the position of the ISM feature. It is very difficult to determine the intrinsic stellar emission line profile, and hence to determine the actual limits of the ISM feature. If the true shape and intensity of the wind lines were known, a more

[4] The Image Reduction and Analysis Facility is distributed by the National Optical Astronomy Observatories, operated by the Association of Universities for Research in Astronomy, Inc., under cooperative agreement with the National Science Foundation.

TABLE 1

INTERSTELLAR AND CIRCUMSTELLAR COMPONENTS TOWARD HD 5980

λ_{obs} (Å) (1)	Line ID (2)	W_λ (mÅ) (3)	V_{hel} (km s^{-1}) (4)	Comments (5)
1152.85.....	P II λ1152.818	103	5	
1153.34.....	P II λ1152.818	69	136[a]	
1153.43.....	P II λ1152.818	6	165[a]	
1155.86.....	C I λ1155.809	8	12	
1161.60.....	Si III* λ1161.58?	7	3:	
1170.03.....	Al II λ1169.846:	20	47:	
1170.44.....	Al II λ1169.846:	8	155:	
1171.05.....	Al II λ1169.846:	5	307:	
1173.32.....	...	14	...	C III DACs?
1174.13.....	...	10	...	C III DACs?
1175.86.....	...	31	...	C III DACs?
1186.90.....	S III λ1190.203	12	−834	
1187.09.....	Si II λ1190.416	8	−841	
1188.03.....	S III λ1190.203	5	−549	
1188.30.....	Si II λ1190.416	4	−536?	
1188.95.....	S III λ1190.203	5	−315?	
1190.21.....	S III λ1190.203	54	3	Plus Si II λ1190.416 at −50 km s^{-1}
1190.45.....	Si II λ1190.416	216	8	Plus S III at 90 km s^{-1}?
1190.76.....	Si II λ1190.416	270	89[a]	Plus S III at 130 km s^{-1}?; 50–240 km s^{-1}
1191.07.....	Si II λ1190.416	380	162[a]	Plus S III at 160 km s^{-1}?
1191.64.....	Si II λ1190.416	24	311	
1191.78.....	Si II λ1190.416	17	343	
1193.06.....	Si II λ1193.290	23	−56	
1193.32.....	Si II λ1193.290	>212	6	
1193.62.....	Si II λ1193.290	202:	82[a]	
1193.94.....	Si II λ1193.290	524:	164[a]	
1194.53.....	Si II λ1193.290	49	309	Plus Si II 1194 at 7 km s^{-1}?
1194.65.....	Si II λ1193.290	20	341	
1194.90.....	Si II* λ1194.500	11:	98[a]	
1195.03.....	Si II* λ1194.500	6:	128[a]	
1195.15.....	Si II* λ1194.500	10:	160[a]	
1195.75.....	Si II* λ1194.500	4:	311:	
1195.86.....	Si II* λ1194.500	16	337	
1197.23.....	Si II* λ1197.394:	21	−44:	$E_1 = 0.04$; but λ1309 absent
1199.41.....	N I λ1199.550	6:	−35	
1199.58.....	N I λ1199.550	179:	9	
1199.90.....	N I λ1199.550	78	88[a]	Partly resolved
1200.09.....	N I λ1199.550	285:	137[a]	
1200.28.....	N I λ1199.550	104:	183[a]	Plus N I λ1200.223 at Galactic velocity
1200.58.....	N I λ1200.223	94	88	
1200.72.....	N I λ1200.223	139:	124[a]	
1200.86.....	N I λ1200.223	123:	158[a]	Plus N I λ1200.710 at Galactic velocity
1201.07.....	N I λ1200.710	82	91[a]	
1201.22.....	N I λ1200.710	119:	129[a]	
1201.34.....	N I λ1200.710	119:	160[a]	
1201.68.....	...	11	...	
1206.56.....	Si III λ1206.500	298:	−5	−45 to +53 km s^{-1}
1207.08.....	Si III λ1206.500	685	⟨150⟩	64–220 km s^{-1}
1207.76.....	Si III λ1206.500	184:	312	
1207.89.....	Si III λ1206.500	80:	343	
1239.50.....	N V λ1238.821	32	⟨169⟩	100–200 km s^{-1}
1239.96.....	Mg II λ1239.925	31	8	
1240.45.....	Mg II λ1239.925	33	127[a]	Plus Mg II 1240 at +10 km s^{-1}
1240.57.....	Mg II λ1239.925	20	156[a]	
1240.92.....	Mg II λ1240.395	8	129[a]	
1241.02.....	Mg II λ1240.395	19	151[a]	
1243.50.....	N V λ1242.804	15	⟨167⟩	90–214 km s^{-1}
1244.08.....	N V λ1242.804	34	⟨310⟩	250–350 km s^{-1}
1250.62.....	S II λ1250.584	88	9	
1250.96.....	S II λ1250.584	25	90[a]	
1251.13.....	S II λ1250.584	67	130[a]	110–190 km s^{-1}
1251.24.....	S II λ1250.584	67	156[a]	
1251.85.....	S II λ1250.584	1	305::	

TABLE 1—*Continued*

λ_{obs} (Å) (1)	Line ID (2)	W_λ (mÅ) (3)	V_{hel} (km s^{-1}) (4)	Comments (5)
1253.85.....	S II λ1253.811	114	9	
1254.19.....	S II λ1253.811	39	88[a]	
1254.35.....	S II λ1253.811	94	126[a]	110–190 km s^{-1}
1254.47.....	S II λ1253.811	97	164[a]	
1255.13.....	S II λ1253.811	1	316::	
1259.56.....	S II λ1259.519	137	8	
1259.88.....	S II λ1259.519	49	86[a]	
1260.12.....	S II λ1259.519	275	142[a]	Plus Si II λ1260.4 at −53 km s^{-1}?
1260.48.....	Si II λ1260.422	290	10	Plus Fe II λ1260.54?
1261.02.....	Si II + Fe II + C I	752	...	Strong, saturated blend
1261.72.....	Si II λ1260.422	92	310	
1261.86.....	Si II λ1260.422	30	340	
1264.50.....	Si II* λ1264.737	2	−53	
1265.20.....	Si II* λ1264.737	5:	111[a]	
1265.30.....	Si II* λ1264.737	4:	135[a]	
1265.41.....	Si II* λ1264.737	12:	159[a]	
1266.09.....	Si II* λ1264.737	12	320	
1266.18.....	Si II* λ1264.737	4	347	
1270.28.....	C I λ1270.143:	7	33::	
1270.59.....	C I λ1270.143:	7	107::	
1277.31.....	C I λ1277.245	33	14	
1277.59.....	C I λ1277.245	2	80	
1277.81.....	C I λ1277.245	4	132[a]	
1277.89.....	C I λ1277.245	7	153[a]	
1280.19.....	C I λ1280.135	10	13	
1280.78.....	C I λ1280.135	4	155	Broad
1284.26.....	Al I λ1284.464:	5	−46:	But no other Al I lines present
1284.62.....	Al I λ1284.464:	2	37:	
1284.69.....	Al I λ1284.464:	<1	52:	
1285.04.....	Al I λ1284.464:	<1	134:	
1285.10.....	Al I λ1284.464:	2	147:	
1285.26.....	Al I λ1284.464:	2	185:	
1297.40.....	...	5	...	
1298.74.....	...	4	...	
1301.92.....	P II λ1301.87	16	10	Plus O I λ1301 at −50 km s^{-1}?
1302.21.....	O I λ1302.168	222	8	Plus P II at $v > 60$ km s^{-1}?
1302.57.....	O I λ1302.168	228:	80[a]	46–225 km s^{-1}
1302.87.....	O I λ1302.168	386:	150[a]	
1303.04.....	O I λ1302.168	47	198[a]	
1303.53.....	O I λ1302.168	7	313	
1304.11.....	Si II λ1304.370:	2	−59:	
1304.40.....	Si II λ1304.370	194	8	
1304.73.....	Si II λ1304.370	67	84[a]	
1304.86.....	Si II λ1304.370	241	114[a]	
1305.09.....	Si II λ1304.370	253	166[a]	
1305.24.....	Si II λ1304.370	22:	197[a]	
1305.72.....	Si II λ1304.370	13	310	
1305.84.....	Si II λ1304.370	4	338	
1317.25.....	Ni II λ1317.217	36	8	
1317.66.....	Ni II λ1317.217	15	96	
1317.78:	Ni II λ1317.217	21	126[a]	
1317.89:	Ni II λ1317.217	32	153[a]	
1318.61.....	Ni II λ1317.217	1	309::	
1318.74.....	Ni II λ1317.217	3	347	
1328.89.....	C I λ1328.834	21	11	
1329.16.....	C I λ1328.834	5	73:	Plus C I* λ1329.10 at 10 km s^{-1} + emission at 101
1329.50.....	C I λ1328.834	2	147	
1334.58.....	C II λ1334.53	293	12	
1335.18.....	C II λ1334.53	830	⟨135⟩	46–240 km s^{-1}
1335.76.....	C II* λ1335.71	138	10	
1335.92.....	C II λ1334.53	80:	313	
1336.08.....	C II* λ1335.71	89:	84[a]	
1336.25.....	C II* λ1335.71	119	128[a]	100–200 km s^{-1}
1336.41.....	C II* λ1335.71	178	159[a]	
1337.10.....	C II* λ1335.71	88	312	

TABLE 1—*Continued*

λ_{obs} (Å) (1)	Line ID (2)	W_λ (mÅ) (3)	V_{hel} (km s^{-1}) (4)	Comments (5)
1337.24.....	C II* λ1335.71	28	341	
1341.16.....	?	5	0	Relative velocities
1341.78.....	?	2	137	Relative velocities
1341.86.....	?	2	154	Relative velocities
1342.58.....	?	1	316	Relative velocities
1342.58.....	Be I λ1342.208:	2	83:	
1356.42.....	O I λ1355.60	2	180	
1347.30.....	Cl I λ1347.239	6	14	
1347.60.....	Cl I λ1347.239	<1	81	
1347.90.....	Cl I λ1347.239	3	147	
1349.32.....	...	4	...	
1355.49.....	O I λ1355.60	2	−25:	
1355.64.....	O I λ1355.60	4	8	
1356.42.....	O I λ1355.60	2	180	
1370.17.....	Ni II λ1370.132	41	6	
1370.55.....	Ni II λ1370.132	7	91	
1370.74.....	Ni II λ1370.132	9	131[a]	
1370.85.....	Ni II λ1370.132	18	166[a]	
1371.54.....	Ni II λ1370.132	3	309	
1371.74.....	Ni II λ1370.132	1:	351:	
1389.88.....	Si IV λ1393.755	15	−836	
1390.84.....	Si IV λ1393.755	24	−630	
1391.28.....	Si IV λ1393.755	53	−534	
1392.37.....	Si IV λ1393.755	12	−298	
1393.76.....	Si IV λ1393.755	99	1[a]	
1393.88.....	Si IV λ1393.755	72	29[a]	
1394.29.....	Si IV λ1393.755	209	116[a]	70–214 km s^{-1}
1394.53.....	Si IV λ1393.755	231	167[a]	
1395.22.....	Si IV λ1393.755	39	315	
1395.34.....	Si IV λ1393.755	3:	342	
1396.97.....	...	8	...	
1398.86.....	Si IV λ1402.770	4	−835	
1399.88.....	Si IV λ1402.770	8	−619	
1400.28.....	Si IV λ1402.770	30	−532	
1401.37.....	Si IV λ1402.770	20	−300	
1402.78.....	Si IV λ1402.770	74	3[a]	
1402.91.....	Si IV λ1402.770	48	30[a]	
1403.29.....	Si IV λ1402.770	154	113[a]	70–214 km s^{-1}
1403.53.....	Si IV λ1402.770	235	162[a]	
1404.22.....	Si IV λ1402.770	27	313	
1404.38.....	Si IV λ1402.770	<1	342	
1445.56.....	...	6	...	
1447.32.....	CO λ1447.36:	1	−8:	
1447.50.....	CO λ1447.36	1	28	
1447.75.....	CO λ1447.36	5	82	
1448.02.....	CO λ1447.36	1	137	
1448.90.....	CO λ1447.36	1	318:	
1454.60.....	Ni II λ1454.842	1	−54	
1454.88.....	Ni II λ1454.842	16	3	
1455.32.....	Ni II λ1454.842	1:	100	
1455.51.....	Ni II λ1454.842	4	133[a]	
1455.59.....	Ni II λ1454.842	8	149[a]	
1456.42.....	Ni II λ1454.842	5:	318	Broad, probably 312 + 340 km s^{-1}
1463.62.....	Ni II λ1467.756:	3	−849:	
1467.79.....	Ni II λ1467.756	11	6	
1468.20.....	Ni II λ1467.756	2	88	
1468.48.....	Ni II λ1467.756	4	145	
1468.54.....	Ni II λ1467.756	2	157	
1526.75.....	Si II λ1526.707	220	10	
1527.38.....	Si II λ1526.707	611	131[a]	50–220 km s^{-1}
1527.70.....	Si II λ1526.707	93::	200[a]	
1527.87.....	Si II λ1526.707	18	228:	
1528.29.....	Si II λ1526.707	22	313	
1528.45.....	Si II λ1526.707	10	344	
1532.60.....	P II λ1532.533	8	12	

TABLE 1—*Continued*

λ_{obs} (Å) (1)	Line ID (2)	W_λ (mÅ) (3)	V_{hel} (km s^{-1}) (4)	Comments (5)
1533.24.....	P II λ1532.533	7	140	
1533.48.....	Si II* λ1533.431	3	10	
1546.44.....	C IV λ1550.772	74	−840	
1547.60.....	C IV λ1550.772	106	−610	
1548.04.....	C IV λ1550.772	344:	−532	Difficult to measure because on wing of steep P Cygni profile
1548.27.....	C IV λ1548.187	350:	10	
1548.98.....	C IV λ1548.187	456:	147	
1549.79.....	C IV λ1548.187	106	306	
1550.77.....	C IV λ1550.772	42	0	
1550.88.....	C IV λ1550.772	191	22	
1551.57.....	C IV λ1550.772	354	156	
1552.36.....	C IV λ1550.772	59	310	
1560.38.....	C I λ1560.309	30	12	
1560.76.....	C I λ1560.309:	11	86:	Plus C I* λ1560.7 (two lines) at +9 km s^{-1}
1560.98.....	C I λ1560.309:	3	128	
1561.11.....	C I λ1560.309:	5	152	
1561.50.....	C I λ1561.44	10	9	Plus C I* λ1560.7 at 152 km s^{-1}
1580.69.....	...	7	...	
1608.14.....	Fe II λ1608.451	3	−56	
1608.49.....	Fe II λ1608.451	182	8	
1608.94.....	Fe II λ1608.451	131	92	
1609.15:	Fe II λ1608.451	147	129[a]	110–190 km s^{-1}
1609.31:	Fe II λ1608.451	151	157[a]	
1609.52:	Fe II λ1608.451	27:	192:	
1610.09.....	Fe II λ1608.451:	7	307	
1610.33.....	Fe II λ1608.451	10	350	
1611.25.....	...	16	...	Sharp line; gfwhm[b] = 13 km s^{-1}
1612.04.....	...	6	...	Sharp line; gfwhm[b] = 10 km s^{-1}
1656.33.....	...	8	...	
1656.99.....	C I λ1656.929	55	11	
1657.44.....	C I λ1656.929	8	92	
1657.63.....	C I λ1656.929	7	127	
1657.76.....	C I λ1656.929	17	149	
1658.19.....	C I* λ1658.121	4	11	
1670.82.....	Al II λ1670.787	251:	7	
1671.30.....	Al II λ1670.787	...	90:	
1671.68.....	Al II λ1670.787	...	...	Highly saturated 88–192 km s^{-1}
1671.92.....	Al II λ1670.787	151	202	gfwhm[b] = 58 km s^{-1}
1672.51.....	Al II λ1670.787	65	310	

NOTE.—Velocities enclosed by angle brackets refer to the average velocity obtained from the flux integration over the line profile without any Gaussian fitting.

[a] Velocities and equivalent widths are obtained from lines that were deblended using multiple Gaussian fits.

[b] Gaussian full width at half-maximum.

precise estimate of the equivalent widths would be possible. However, in the case of HD 5980, it would be premature to construct a theoretical line profile to use as a template for the wind lines in order to measure the ISM features because there are several stars contributing to the wind features, in addition to the possibility of a contribution from a stellar wind-wind collision zone (Moffat et al. 1998), and the lines are highly variable. Hence, at this stage, we opted for merely performing a visual interpolation across the ISM features taking into account the presence of the underlying wind lines. A posteriori, we find that the equivalent width of the ISM lines, such as Si IV λ1393, which is superposed on the steep wing of the P Cygni feature, can be underestimated by as much as ∼30%.

The second source of uncertainty is in the deblending process through the use of a small number of Gaussian profiles. For any given feature, we used the smallest number of Gaussians needed to provide a reasonable fit to the line profile, although we are aware (see Welty et al. 1997) that a large number of ISM velocity components probably contribute to each absorption feature.

In Table 1, we list the results of the measurements. Column (1) contains the wavelength of the measured absorption; column (2) lists the line identification, with the reference wavelength taken from the NIST database; column (3) is the equivalent width of the feature; column (4) is the velocity measured with respect to the laboratory wavelength (i.e., the heliocentric velocity); and column (5) lists comments. Lines with uncertain measurements in Table 1 are indicated by a colon. The primary sources of these uncertainties are (1) a poor fit to a blended line profile; (2) a questionable line indentification; (3) unusual difficulty in placing the continuum level. We estimate the uncertainty in equivalent width measurements to be about 3% for isolated ISM lines (such as the Galactic C I lines) that do not lie on steep portions of stellar wind lines, and

$\sim$10% for blended lines. Velocities and equivalent widths obtained from lines that were deblended using multiple Gaussian fits are footnoted in column (4) of Table 1; velocities enclosed by angle brackets refer to the average velocity obtained from the flux integration over the line profile without any Gaussian fitting.

A few absorption lines were not identified but appear to be real, the most noteworthy of which is the set of lines starting at 1341.16 Å that, although rather weak, suggests an atomic transition present in most of the SMC velocity systems, in addition to the Galactic one.

3. PRINCIPAL VELOCITIES

Using the data in Table 1, we grouped the individual velocities into broad velocity bins and averaged the values within each bin. This yields the following different velocity systems, with their corresponding standard deviations: three components at $v < 80$ km s^{-1} ($V_{\rm hel} = 1.1 \pm 3$, 9 ± 2, 28 ± 3 km s^{-1}), the first two of which are dominated by the contribution from the Galactic disk and halo; seven components in the SMC ($V_{\rm hel} = 87 \pm 6$, 110 ± 6, 132 ± 6, 158 ± 8, 203 ± 15, 312 ± 3, 343 ± 3 km s^{-1}); five circumstellar (CS) velocity systems ($V_{\rm hel} = -1020$, -840, -630, -530, and -300 km s^{-1}) associated with HD 5980; and a possible system at -53 ± 5 km s^{-1} of uncertain origin (seen only in some of the Si II lines and marginally in Fe II).

Table 2 summarizes the heliocentric velocities measured for each of the ISM lines. The first column on the left lists the line ID and the other columns list the measured velocity of each line. The Galactic components are all grouped together under the column labeled "+8." We have, however, explicitly included in this column the +28 km s^{-1} component when detected. The SMC components are listed under their closest principal velocity. As in Table 1, for data footnoted "a" the listed velocity was obtained by deblending a broad feature; for those footnoted "b" the listed velocity is simply the average of the velocity range observed, with a solid line indicating this range, which is in general broader than that given by the principal velocities listed in Table 1. Examples of the line profiles on a velocity scale are presented in Figures 1–4.

Four of our SMC velocity systems coincide within the errors with the four main gas complexes in the SMC at $V_{\rm hel} = 114 \pm 6$, 134 ± 9, 167 ± 8, and 192 ± 8 km s^{-1} that have been identified from a survey of H I 21 cm emission (McGee & Newton 1981, 1982).

The SMC components at +87 km s^{-1} are present in C I, C II, N I, O I, Si II, S II, Fe II, Ni II, Cl I, and CO and, in many cases, can be clearly separated from the 110–220 km s^{-1} blend. Within the 110–220 km s^{-1} blends, we find the strongest contributions at +132 and +158 km s^{-1}, with weaker contributions at +110 and +200 km s^{-1}. Some of the saturated lines, however, reach zero residual intensity in the velocity range $\sim$85–170 km s^{-1} indicating that the column density within the +110 km s^{-1} system is also significant.

We note the presence of C I lines at the SMC velocities (predominantly in the +87, +132, and +158 km s^{-1} complexes), not previously detected in the UV, as well as weak lines such as O I λ1355.

The component at -53 km s^{-1} is visible in Si II $\lambda\lambda$1190, 1193, and 1260, although the Si II 1260 Å line is severely blended with S II λ1259. It is absent in Si II λ1526. If it is related to gas in the SMC, it would be moving at $\sim$200 km s^{-1} with respect to the SMC, a velocity even higher than that of the SNR (see below), but tantalizingly close to the expected outflow velocity from HD 5980 at the time of outburst. The two dotted tracings at the bottom of Figure 1 correspond to the excited transitions of Si II* λ1264 and λ1194, both of which are much weaker that the other lines plotted in this figure, and thus we have rescaled the flux values by a multiplicative factor (indicated in parentheses). Note that the two strongest absorptions in the λ1194 tracing belong to Si II λ1193 (its +311 and +342 components). The strongest absorption in the excited transitions occurs at +160 km s^{-1}. There is an absorption in this wavelength range that, if it were due to Si II* at 1194 Å, would lie at +342 km s^{-1}, but this identification is doubtful.

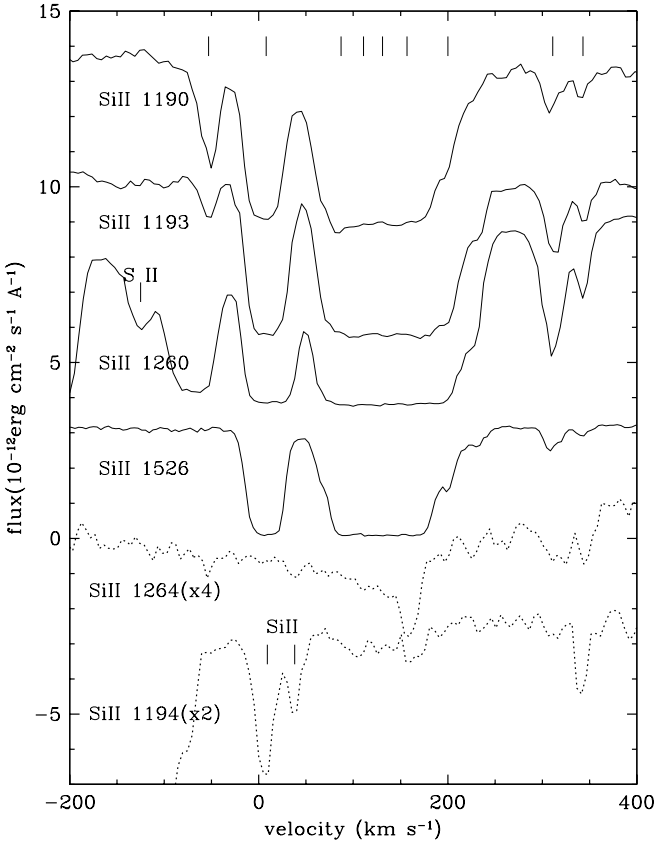

FIG. 1.—Si II lines plotted as a function of velocity. The tick marks indicate the heliocentric velocities of -53, 8, 87, 110, 132, 158, 203, 312, and 343 km s^{-1}. Velocities larger than 70 km s^{-1} correspond to ISM structures in the SMC; the heliocentric velocity with respect to the LSR is 10 km s^{-1}. Tracings have been displaced vertically for clarity. The fluxes of the lines at 1264 and 1194 Å have been scaled by the value shown in parenthesis in order to make the (weak) absorption features visible in this figure. These lines arise from the excited lower state ($E_1 = 0.04$ eV).

3.1. *SNR 0057−7226*

The two systems at $+312 \pm 3$ and $+343 \pm 3$ km s^{-1} can be associated with the $v_{\rm LSR} = +300$ km s^{-1} feature first detected by de Boer & Savage (1980) and subsequently attributed to an SNR by Fitzpatrick & Savage (1983). Our detected $V_{\rm hel} = 312$ km s^{-1} component coincides extremely well with the component reported by de Boer & Savage (1980), given that we have $v_\odot = 12$ km s^{-1} with respect to

TABLE 2

VELOCITIES OF ISM FEATURES

LINE	HELIOCENTRIC VELOCITY (km s^{-1})								
	−53	+8	+87	+110	+132	+158	+200	+312	+343
C I λ1155	...	12	...	...	...	...	...	...	...
C I λ1277	...	14	80	...	132[a]	153[a]	...	...	...
C I λ1280	...	13	...	...	...	155	...	...	...
C I λ1328	...	11	73:	...	...	147	...	...	...
C I λ1560	...	12	86:	...	128	152	...	...	...
C I λ1561	...	9:	...	...	...	...	...	...	...
C I λ1656	...	11	92	...	127	149	...	...	...
C I* λ1658	...	11	...	...	...	...	...	...	...
C II λ1334	...	12	———		135	———		313	...
C II* λ1335	...	10	84	...	128[a]	159[a]	...	312	341
C IV λ1548	...	10	...	...	...	147	...	306	...
C IV λ1550	...	0+22	...	...	...	156	...	310	...
N I λ1199	−35	9	88	——	137[a]	183:[a]	——	...	...
N I λ1200.2	...	...	88	——	124[a]	158[a]	...	...	...
N I λ1200.7	...	...	91	——	129[a]	160[a]	...	...	...
N V λ1238	...	...	...	———		160[b]	——	...	...
N V λ1242	...	...		———		167[b]	——	310[b]	...
O I λ1302	...	8	80[a]			150[a]	198[a]	313	...
O I λ1355	−25	8	...	...	...	...	180	...	...
Mg II λ1239	...	8	...	...	127	156	...	...	...
Mg II λ1240	...	...	...	...	129	151	...	...	...
Al II λ1670	...	7	90:	———				310	346
Si II λ1190	...	8	89[a]	———		162[a]	——	311	343
Si II λ1193	−56	6	82[a]	———		164[a]	——	309	341
Si II λ1260	...	10	...	———				310	340
Si II λ1304	−59:	8	84[a]	114[a]	——	166[a]	197[a]	313	342
Si II λ1526	...	10	———		131[a]	——	200[a]	313	344
Si II* λ1194	...	...	98[a]	——	128[a]	160[a]	...	311	337
Si II* λ1197	−44	...	...	...	...	...	...	...	...
Si II* λ1264	−53	...	...	111	135	159	...	320	347
Si III λ1206	...	−5+30	...	———				312	343
Si III* 1161:	...	3:	...	...	...	...	...	...	...
Si IV λ1393	...	1+29	——	116[a]	——	167[a]	——	315	342:
Si IV λ1402	...	3+30	——	113[a]	——	162[a]	——	313	342:
P II λ1152	...	5	———		136[a]	165[a]	...	...	...
P II λ1301	...	10	...	...	...	...	...	...	...
P II λ1532	...	12	...	...	140	——	...	...	...
S II λ1250	...	9	90	——	130[a]	156[a]	...	305::	...
S II λ1253	...	9	88	——	126[a]	164[a]	...	316::	346::
S II λ1259	...	8	86	...	142	...	...	...	...
S III λ1190	...	3:	...	...	...	...	...	...	...
Fe II λ1608	−56	8	92	——	129[a]	157[a]	192:	307	350
Ni II λ1317	...	8	96	——	126[a]	153[a]	...	309:	347
Ni II λ1370	...	6	91	——	131[a]	166[a]	...	309	351:
Ni II* λ1454	−54	3	...	100	133[a]	149[a]	...	318[b]	...
Ni II* λ1467	...	6	88	...	145	157	...	...	...
Be I λ1342	...	...	83:	...	...	...	...	...	...
Cl I λ1347	...	14	81	...	147	...	190	...	...
CO λ1447	...	−8:, 28	82	...	137	...	...	318:	...

[a] Velocities and equivalent widths are obtained from lines that were deblended using multiple Gaussian fits.

[b] Velocities are the average of the velocity range observed.

the v_{LSR} from the C I and C I* velocities listed in Table 2 (excluding λ1561). The second component, however, was not detected by these authors, probably because it is weaker. Both absorptions arise in gas that is receding from the observer and approaching HD 5980. It is interesting to note that there is a correlation between the strength of the +312 and +343 km s^{-1} components and the degree of blending between the +87 km s^{-1} and the Galactic absorption blend: When the SNR components are weak or absent, the Galactic absorption is well separated from the SMC components, and the intervening spectral region approaches the continuum level. Conversely, lines having very strong SNR components are associated with more absorption in the intervening spectral region between the Galactic and SMC components. The most extreme case is Si III λ1206, as illustrated in Figure 5, where we compare Si II, Si III, and Si IV lines with the S II 1250 Å line, which has no significant contribution from the SNR. This effect sug-

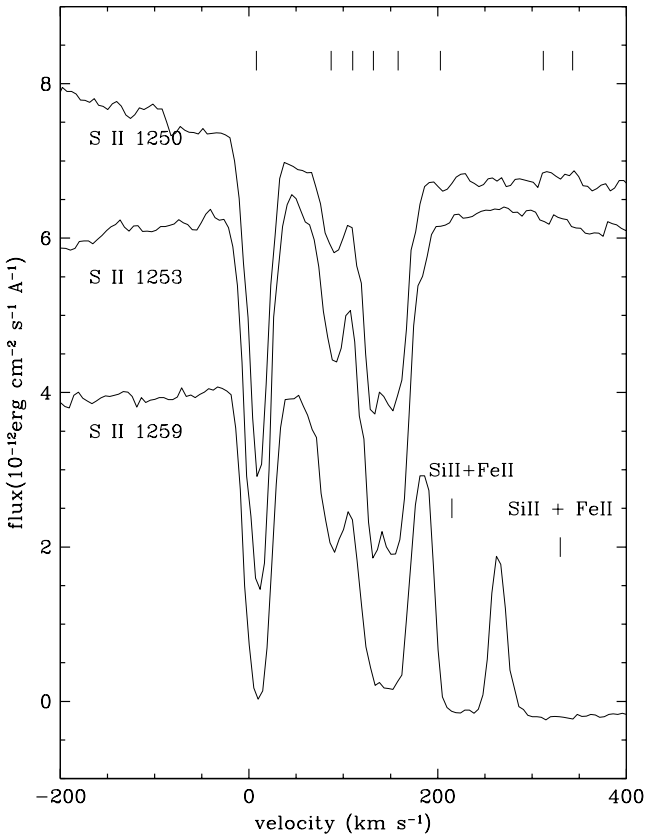

FIG. 2.—Same as Fig. 1, but for S II lines

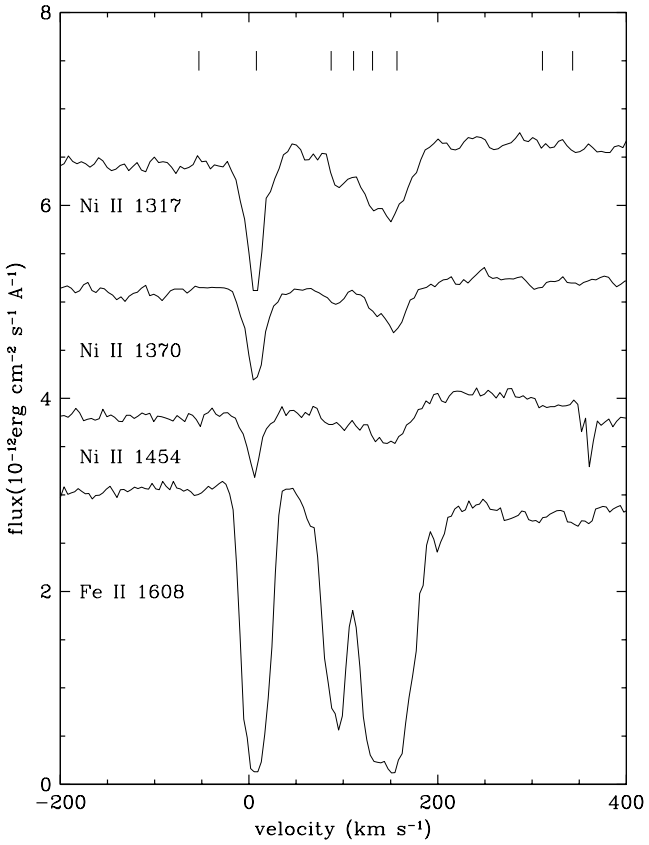

FIG. 3.—Fe II 1608 Å and Ni II lines plotted as a function of velocity. Tick marks indicate principal velocities as described in Fig. 1. Plots are displaced vertically for clarity.

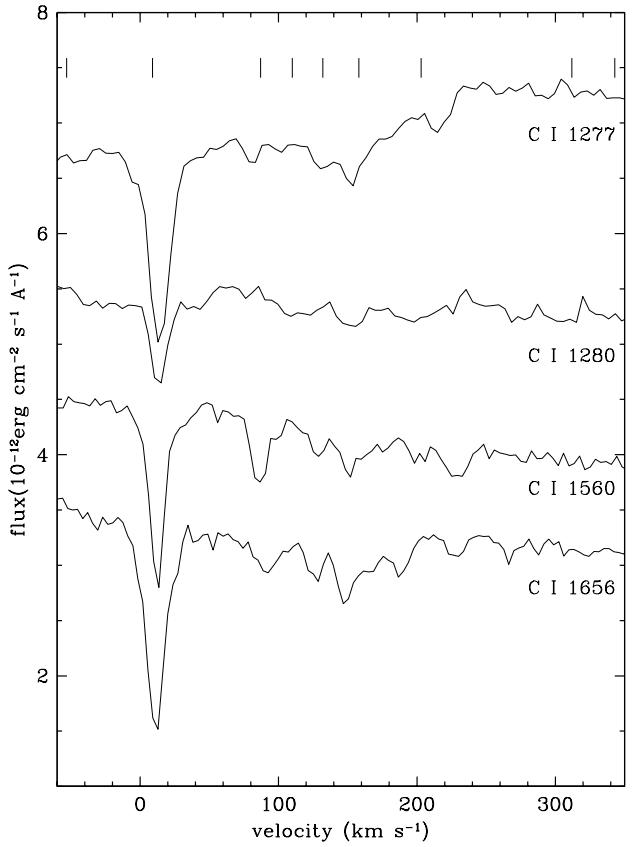

FIG. 4.—Same as Fig. 1, but for C I lines

gests that the wavelength range between the Galactic and the SMC velocity systems (i.e., between ~ 8 and ~ 80 km s^{-1}) contains a contribution from the approaching portion of the SNR shell. Indeed, after subtracting the profile of Si III λ1206 from Si II λ1526 (which does not have evident $+312$ and $+343$ absorption components) excess absorption appears at two velocities: $+33$ and $+64$ km s^{-1}. This is illustrated in Figure 6. The velocity of $+33$ km s^{-1} coincides within the errors with the component at roughly $+28$ km s^{-1} that is prominent particularly in Si IV and C IV, as well as Si III. Hence we can now associate this component with the approaching portion of the SNR. Assuming that each pair of velocities ($+33$, $+343$) and ($+64$, $+312$) corresponds to one of two approaching and two receding velocity systems associated with the SNR, the same systemic velocity is found from both pairs: $v_{\rm SNR} = +188$ km s^{-1}, assuming that the expansion of the SNR is symmetric. This velocity lies within the range of velocities $+180$ to $+220$ km s^{-1} that we obtain from *HST* archival spectra of four of the O3–O6 stars in NGC 346 (NGC 346-113, -324, -355, -368; number IDs from Massey, Parker, & Garmany 1989). Hence, it is very likely that the progenitor of SNR 0057−7226 was one of the most massive stars formed in the NGC 346 cluster, assuming coeval star formation.

Two final points that should be made are that (1) it is interesting to note the detection of CO at 1447 Å at $+28$ km s^{-1} and possibly at $+318$ km s^{-1}, raising the question of its possible association with the SNR; (2) the Galactic ISM components are partially contaminated by the SNR and may also contain absorption arising in slowly moving ejecta of HD 5980.

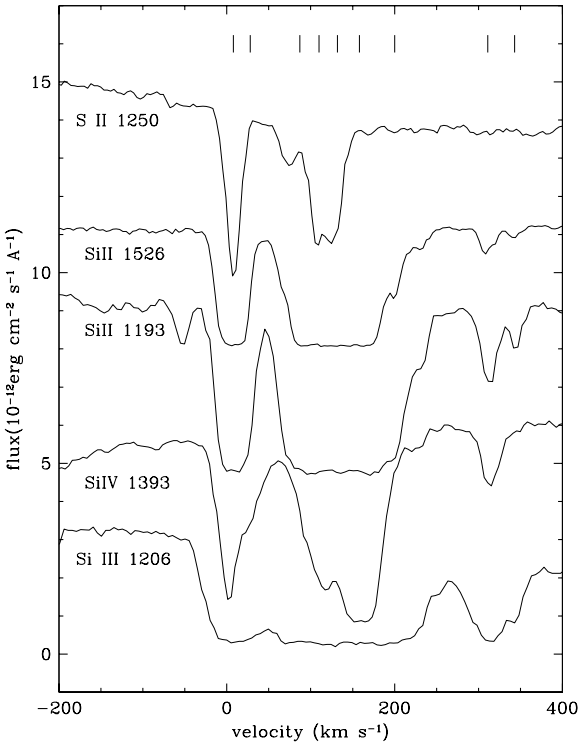

FIG. 5.—Montage of Si II, Si III, and Si IV lines compared with S II λ1250. The SNR absorption components are strongest in the Si III line, which also shows the most severe blending between the Galactic components and those arising in the SMC, implying the presence of SNR absorptions due to the approaching portion of the shell in the velocity range 10–80 km s^{-1}. The tick marks are set at V_{hel} = 8, 28, 87, 110, 132, 158, 203, 312, and 343 km s^{-1}.

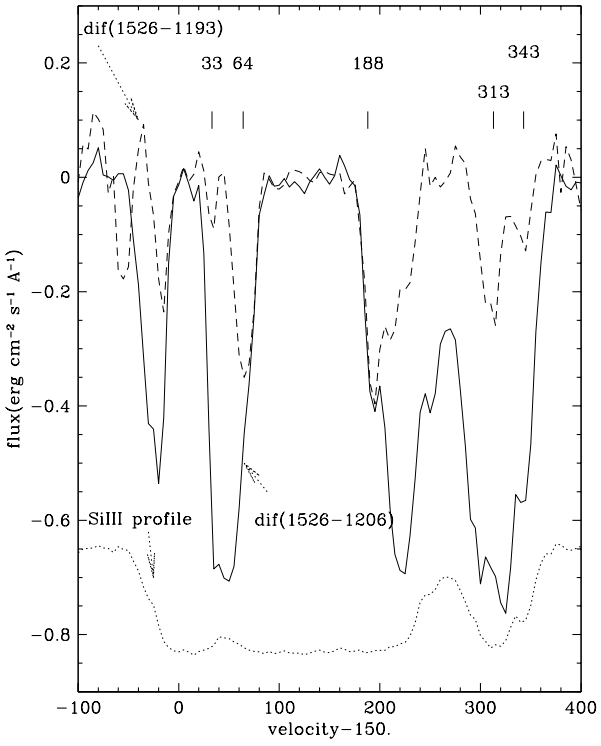

FIG. 6.—Differences between the Si II 1526 Å line and the Si II 1193 Å line (*dashed tracing*), and between Si II λ1526 and Si III λ1206 (*solid tracing*). The dotted tracing is the Si III λ1206 line profile, rescaled and shifted down, for illustration purposes. Note the components at +33 and +64 km s^{-1}, which most likely correspond to the +343 and +312 km s^{-1} SNR components.

3.2. *Very High Velocity Circumstellar Components*

Absorption features that we attribute to circumstellar gas are illustrated in Figures 7 and 8, where we plot, respectively, the two lines of Si IV (λλ1393 and 1402) and C IV λ1550, observed in the 1999 and the 2000 data. Tick marks at the top of each panel indicate the values of the CS velocities in 1999, as well some of the other ISM components. The various components are much easier to identify in the Si IV lines because of the larger separation between the wavelengths of the doublet. The most prominent of the CS components lies at $V_{hel} = -533 \pm 2$ km s^{-1} in 1999. One year later, this component becomes broader, giving the appearance of a second component that has developed at a veloc-

TABLE 3

COMPARISON OF 1999 AND 2000 HIGH-VELOCITY FEATURES IN Si IV

	1999					2000				
LINE	λ_{obs} (Å)	W_λ (mÅ)	log N(cm^{-2})	V_{hel} (km s^{-1})	gfwhm (km s^{-1})	λ_{obs} (Å)	W_λ (mÅ)	log N(cm^{-2})	V_{hel} (km s^{-1})	gfwhm (km s^{-1})
Si IV 1393.755.....	1388.97	93	13.02	−1020	124	1388.53	104	13.07	−1126	67
	1389.88	15	12.23	−836	25	1389.76	15	12.23	−860	27
	1390.84	24	12.43	−630	43	1390.57	5	11.75	−685	13
	...	...	...	...	...	1391.09	43	12.68	−573	27
	1391.28	53	12.78	−534	26	1391.22	34	12.58	−546	27
	...	...	...	...	...	1392.18	18	12.31	−338	24
	1392.37	12	12.13	−298	32	1395.22	36	12.61	−314	22
Si IV 1402.770.....	1397.97	73	13.21	−1021	118	1397.53	44	12.99	−1125	55
	1398.86	4	11.95	−835	28	1398.76	14	12.50	−860	23
	1399.88	8	12.25	−619	34	...	...	...	...	...
	...	...	...	...	...	1400.09	34	12.88	−574	29
	1400.28	30	12.83	−532	22	1400.24	14	12.50	−542	18
	...	...	...	...	...	1401.17	11	12.39	−344	22
	1401.37	20	12.65	−300	32	1404.23	26	12.77	−310	28

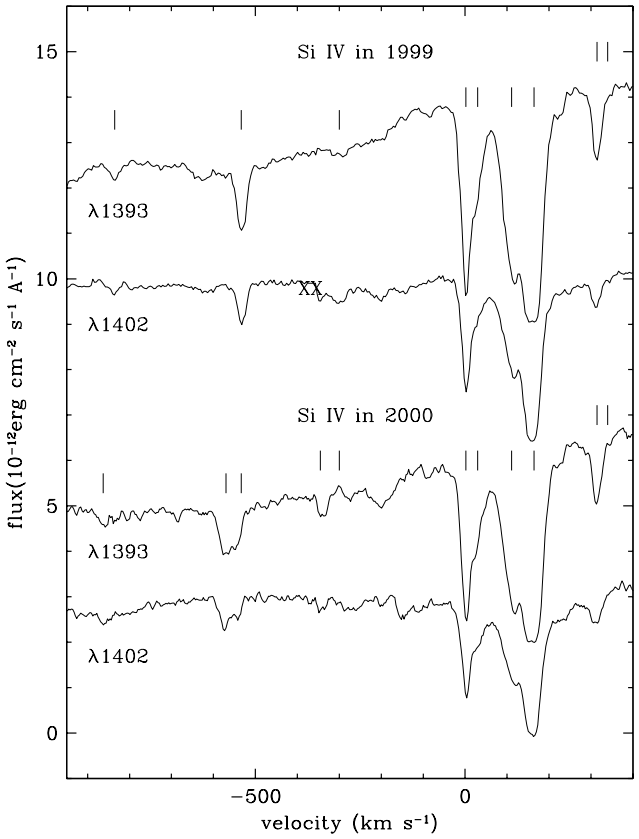

FIG. 7.—Comparison of the high-velocity circumstellar components of Si IV in spectra obtained in 1999 and in 2000. The tick marks on the top of the figure mark features at −839, −533, and −300 km s^{-1} arising either in the circumstellar or wind material of HD 5980. Also marked are the principal Galactic components at 2 and 30 km s^{-1}; and the SMC components at 110, 158, and 312 km s^{-1}. The same features are noted on top of the 2000 spectrum, with the changes in the high-velocity components also indicated. Note that the SMC component at 343 km s^{-1} is nearly undetectable in Si IV, while it is quite strong in Si II (Fig. 5). The label "XX" marks the position of a blemish on the data.

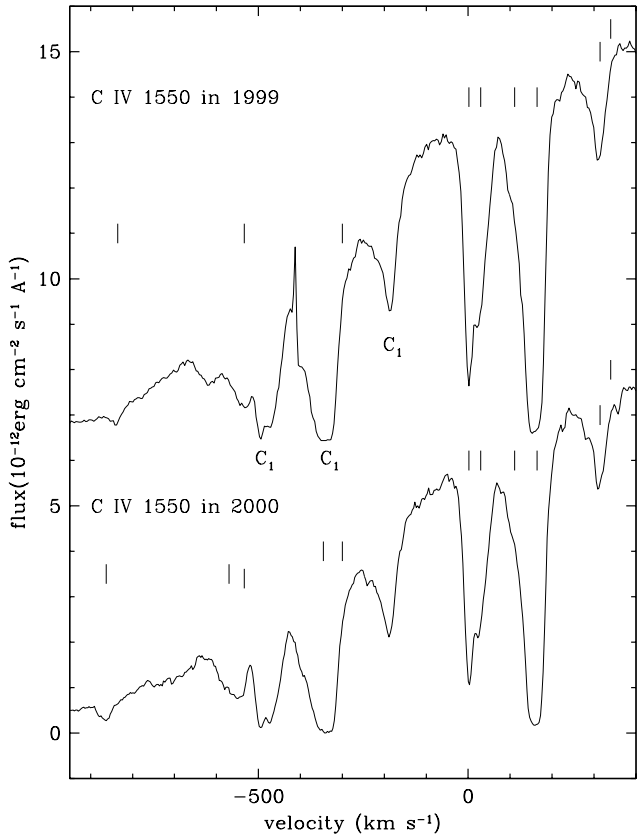

FIG. 8.—Same as Fig. 7, but for C IV λ1550. The circumstellar or wind components of the C IV 1548 Å line lie deep within the P Cygni profile, but some absorptions are visible. The lower tracing is unshifted and the upper tracing is shifted by 6.5 in the vertical scale. The strong absorptions labeled "C_1" are the 2 + 28, 110 + 158, and 312 km s^{-1} features belonging to C IV λ1548.

ity −50 km s^{-1} faster than the first one. A similar trend is visible in the other CS features of Si IV and in C IV, although the blending of the various velocity systems of the two C IV lines makes them more difficult to identify. Additional lines that probably display these high-velocity CS features are Si II λ1190.4, S III λ1190.2, and possibly Ni II λ1467. The characteristics of the Si IV absorption components in 1999 and 2000 are presented in Table 3.

4. COLUMN DENSITIES

Column densities were obtained through two different methods. For all the measured lines, we estimated the column densities assuming that the lines are optically thin, using

$$N(\mathrm{cm}^{-2}) = 1.13 \times 10^{17} \frac{W_\lambda(\mathrm{mÅ})}{f\lambda^2(\mathrm{Å})} \quad (1)$$

(Spitzer 1978, p. 51), where f is the oscillator strength (see Morton 1991 for a recent compilation). This assumption is valid if each observed absorption consists of a blend of undamped individual lines. The recent Australia Telescope Compact Array H I survey (Staveley-Smith et al. 1997) has resulted in the description of the SMC ISM as consisting of "frothy and filamentary" shell-like structures, suggesting that the optically thin approximation is probably adequate for most of the lines that are not obviously saturated. The second method employed is the classical curve-of-growth method (Spitzer 1978, p. 51) using the lines of Si II, Si II*, Si III, Si IV, N V, C II, C IV, and Al II, yielding column densities for these species in the Galactic, the +312, and the +343 km s^{-1} components.

The values obtained using equation (1) are listed in Table 4, where the first column lists the identification of the absorption line and the other columns list the column densities estimated for each of the velocity components. Lower limits are indicated for the saturated lines, and the colon indicates that the original measurement has a greater uncertainty than the average. The asterisk beside the Galactic values of Si IV indicates that the column density is the combined value of both the ∼0.0 and the +28 km s^{-1} components. The uncertainty in the logarithmic column densities is, in general, ∼0.10 dex for the Galactic components and ∼0.20 dex for the blended SMC features. A conservative estimate of the uncertainties for the SNR logarithmic column densities is ∼0.06 dex. Also, a comparison between the column densities derived from the two components of the Si IV doublet indicates that ISM absorption lines superposed upon the wind emission lines lead to column densities that are being underestimated by 0.2 to 0.3 in the log N value.

Many of the ISM line cores have zero residual intensities over wide ranges in velocity. Examples of these saturated

TABLE 4

COLUMN DENSITIES $\log N(\mathrm{cm}^{-2})$

LINE	HELIOCENTRIC VELOCITY (km s^{-1})								
	−53	+8	+87	+110	+132	+158	+200	+312	+343
C I λ1155	...	13.59	...	...	...	...	...	...	...
C I λ1277	...	13.37	12.16	...	12.46	12.70	...	...	...
C I λ1280	...	13.45	...	...	...	13.05	...	...	...
C I λ1328	...	13.36	12.74:	...	...	12.34	...	...	...
C I λ1560	...	13.24	12.80:	...	12.24	12.46	...	...	...
C I λ1656	...	13.21	12.37	...	12.31	12.70	...	...	...
C II λ1334.....	...	14.16	———		14.61	———	...	13.60:	...
C II* λ1335	...	13.84	13.69:	...	13.82	13.99	...	13.68	13.19
C IV λ1548	...	14.28:	...	...	...	14.40	...	13.77	...
C IV λ1550	...	13.36	...	...	...	14.29	...	13.51	...
N I λ1199	...	14.02:	13.66	...	14.23:	13.79	...	...	...
N I λ1200.2	...	...	13.92	...	14.09:	14.04:	...	...	...
N I λ1200.7	...	...	14.16	...	14.32:	14.32:	...	...	...
N V λ1238	...	...	...	———		13.18	———	...	...
N V λ1242	...	...	...	———		13.15	———	13.50	...
O I λ1302	...	15.22	15.23	...	...	15.46:	14.55:	13.72	...
O I λ1355	...	17.27	...	...	...	...	16.99:	...	...
Mg II λ1239.....	...	15.93	...	...	15.96	15.74	...	...	...
Mg II λ1240.....	...	...	...	...	15.64	16.02	...	...	...
Al II λ1670	...	12.74:	...	...	...	...	...	12.16	11.34
Si II λ1190	...	13.84:	13.93:	...	...	14.08:	...	12.88	12.73
Si II λ1193	12.56	>13.53	13.51:	...	...	13.92:	...	12.89	12.50
Si II λ1260	...	13.31:	...	...	...	...	...	12.81	12.33
Si II λ1304	11.96	13.94	13.48:	14.04	...	14.06	13.00:	12.77	12.26
Si II λ1526	...	13.67	...	...	14.11	...	13.29:	12.67	12.32
Si II* λ1194	...	...	12.14:	...	11.88:	12.10:	...	11.71:	12.31
Si II* λ1197	12.12	...	...	...	...	...	...	...	...
Si II* λ1264	11.19	...	...	11.59:	11.49:	11.97:	...	11.97	11.49
Si III λ1206.....	...	13.14:	———			13.50	———	12.93:	12.57:
Si IV λ1393.....	...	13.05*	...	13.37	...	13.42	...	12.64	<11.53
Si IV λ1402.....	...	13.22*	...	13.54	...	13.72	...	12.78	<11.35
P II λ1152.....	...	13.57	...	...	13.40	12.33	...	...	...
P II λ1301.....	...	13.79	...	...	...	...	...	...	...
P II λ1532.....	...	13.70	...	...	13.64	...	...	...	...
S II λ1250	...	15.07	14.52	...	14.95	14.95	...	13.12:	...
S II λ1253	...	14.88	14.41	...	14.79	14.81	...	12.82:	...
S II λ1259	...	14.77	14.33	...	15.08:	...	...	...	...
S III λ1190	...	14.29	...	...	...	...	...	...	...
Fe II λ1608.....	12.32	14.11	13.97	...	14.02	14.03	13.28:	12.69	12.85
Ni II λ1317.....	...	13.21	12.82	...	12.97	13.16	...	11.65::	12.13
Ni II λ1370.....	...	13.27	12.51	...	12.62	12.92	...	12.14:	11.66
Ni II λ1454.....	11.95	13.16	11.95:	...	12.55	12.86	...	12.65:	...
Ni II λ1467.....	...	13.41	12.66	...	12.97:	12.66	...	...	...
Be I λ1342	...	...	...	...	...	...	...	...	...
Cl I λ1347.....	...	12.50	<11.72	...	...	12.20	...	...	...

profiles include most of the Si II lines (saturated between +87 and +190 km s^{-1}), shown in Figure 1. The deblending process we have applied to these lines serves only as a crude estimate for the equivalent widths. Other lines are clearly not saturated, examples of which are the C I lines illustrated in Figure 4, all components of the Ni II lines (Fig. 3), the components at +87 km s^{-1} in S II and Fe II (Figs. 2 and 3), and all of the components at +312 and +343 km s^{-1}.

In Table 5 we summarize the column densities derived for the Galactic, the SMC, and the +312 and +343 km s^{-1} components from the application of equation (1). The integrated SMC column densities were obtained by adding the equivalent widths of the components listed in Table 1 in the +87 through +200 km s^{-1} velocity bins, and applying equation (1) to this combined value of the equivalent width. The last two columns of this table list the density values obtained by other authors (Welty et al. 1997 for the line of sight toward Sk 108; Savage & de Boer 1981, for the line of sight to HD 5980; and de Boer & Savage 1980, also for the line of sight to HD 5980). Note that the NV lines previously reported as ISM lines may be contaminated by stellar photospheric absorption (see Fig. 9).

We obtain a column density for C I of $\log N(\mathrm{C\ I}) = 13.36 \pm 0.09$ s.d. from four lines at the Galactic velocity and $\log N(\mathrm{C\ I}) = 12.99 \pm 0.04$ s.d. from three lines in the SMC. The SMC lines lie in the +132 to +158 km s^{-1} range of velocities.

The Galactic O I line at 1355.60 Å is definitely present, and although it lies on the descending wing of a P Cygni absorption component, the definition of the local contin-

TABLE 5

INTEGRATED COLUMN DENSITIES log $N(\mathrm{cm}^{-2})$

	This Paper					Other Authors	
Line	−53	Gal.	SMC	+311	+343	Gal.	SMC
C I λ1277	...	13.37	12.97	...	...	...	...
C I λ1280	...	13.45	13.05	...	...	...	...
C I λ1328	...	13.36	...	...	...	13.40[a]	<13.00[a]
C I λ1560	...	13.24	13.04	...	...	...	...
C I λ1656	...	13.21	12.97	...	...	...	...
C II λ1334.....	...	14.16	>14.61	13.60:	...	...	...
C II1335[b]	...	13.84	14.33	13.68	13.19	...	...
C IV λ1548	...	14.28:	14.40	13.77	...	...	14.35[c]
C IV λ1550	...	13.36	14.29	13.51	...	...	...
N I λ1199	...	14.02:	>14.44	...	...	...	...
N I λ1200.2	...	...	>14.50	...	...	...	...
N I λ1200.7	...	...	>14.75	...	...	...	...
N V λ1238	...	...	13.18:	...	...	...	...
N V λ1242	...	...	13.15:	13.50:	...	...	13.54[c]
O I λ1302	...	>15.22	>15.70	13.72	...	...	...
O I λ1355	...	17.29	16.87:	...	...	...	...
Mg II λ1239.....	...	15.93	16.16	...	...	...	...
Mg II λ1240.....	...	...	16.17	...	...	...	...
Si II λ1193	12.56	>13.53	14.06	12.89	12.50	...	...
Si II λ1304	11.96	>13.94	>14.42	12.77	12.26	>14.45[a]	>14.89[a]
Si II λ1526	...	13.67	14.18	12.67	12.32	...	...
Si II λ1194[b]	...	...	12.53	11.71:	12.31	<12.0[a]	<12.38[a]
Si III λ1206.....	...	13.14:	13.50	12.93:	12.57:	...	...
Si IV λ1393.....	...	13.05[b]	13.70	12.64	...	...	~13.8[d]
Si IV λ1402.....	...	13.22[b]	13.94	12.78	<11.35	...	...
P II λ1152.....	...	13.57	13.43	...	...	13.97[a]	...
S II λ1250	...	15.07	>15.32	...	...	>15.20[a]	>15.26[a]
S II λ1253	...	14.88	>15.18	...	...	>15.00[a]	>15.20[a]
S II λ1259	...	14.77:	> 15.15	...	...	bl	bl
S III λ1190	...	14.29	...	...	...	...	...
Fe II λ1608.....	12.32	14.11	14.51	12.69	12.85	14.78[a]	14.84[a]
Ni II λ1317.....	...	13.21	13.48	...	...	13.18[a]	13.08[a]
Ni II λ1370.....	...	13.27	13.67	...	...	...	...
Ni II λ1454.....	11.95	13.16	13.07::	12.65:	...	...	...
Ni II λ1467.....	...	13.41	13.27::	...	...	...	...

NOTES.—The Galactic component of C IV λ1548 contains the contribution from the +28 km s^{-1} component, while that of C IV λ1550 does not. C IV λ1548 is more difficult to measure given its position near the base of the wing of a P Cygni absorption component.

[a] Welty et al. 1997.

[b] Column density includes the +28 km s^{-1} component.

[c] Savage, Sembach, & Lu 1997

[d] Savage & de Boer 1981.

uum level is relatively straightforward. Its measured equivalent width is $W_\lambda = 4 \pm 0.4$ mÅ, which yields a column density $\log N(\mathrm{O\ I}) = 17.29 \pm 0.05$ for the Galactic component. The possible SMC component, if real, lies at +180 km s^{-1} and we derive a column density $\log N(\mathrm{O\ I}) = 16.87 \pm 0.15$, where the uncertainty refers only to the error in the continuum placement. The actual equivalent width of this feature ($W_\lambda = 1.5 \pm 0.5$ mÅ) is near the noise level of the data.

Column densities of selected lines for the Galactic and the +312 and +343 km s^{-1} components were also obtained through the construction of curves of growth for these observed lines, and comparison of the theoretical curve of growth constructed following Spitzer (1978, p. 51). The curve of growth for the +312 km s^{-1} and the Galactic absorption components are illustrated in Figures 10*a* and 10*b*, where the different symbols correspond to the different lines used. The formal uncertainty in the $\log N$ value for these column densities is ±0.02. A comparison between the values obtained through the use of equation (1) and the curve-of-growth method is presented in Table 6. The largest differences between the two methods occur for the saturated lines, as would be expected because of the optically thin assumption inherent to equation (1).

For the SNR components at +312 and +343 km s^{-1}, we obtain ratios of column densities of Si II/Si III/Si IV = 1.0/~2.5/0.4 and 1.0/1.1/0.0, respectively, values that can be compared with the Galactic component, for which Si II/Si III/Si IV = 1.0/0.6/0.01. This implies that the +312 km s^{-1} component has a very different ionization balance from the +343 km s^{-1} component and the average Galactic component, as would be expected from an SNR, in which collisional processes dominate. The electron temperature for the SNR implied by these ratios is $T_e \sim 40{,}000$ K (Baliunas & Butler 1980). Also, from a comparison of the observed ratios Si II/Si II* ~ 1/10 and C II/C II* ~ 1/1 with

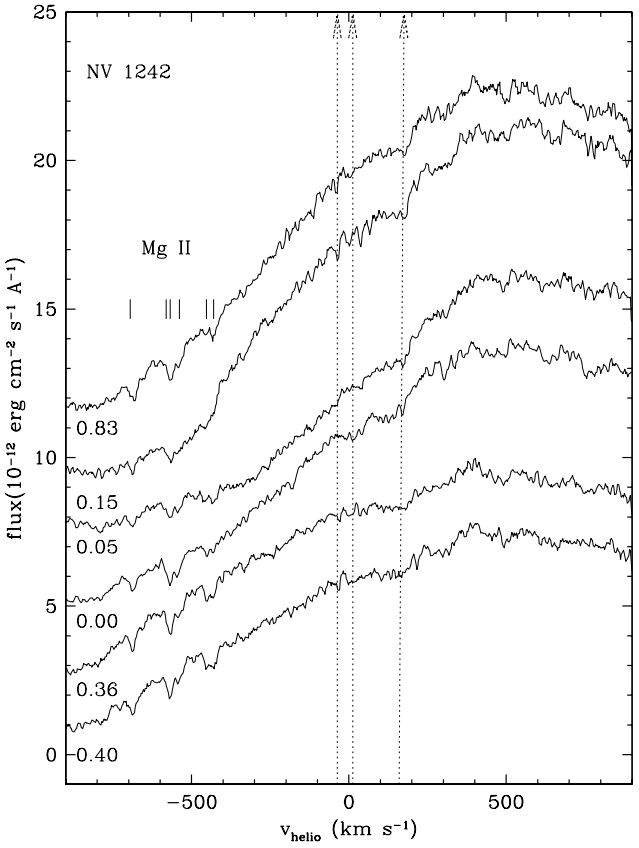

FIG. 9.—Montage of the six individual N v λ1240 line profiles on a velocity scale. The orbital phase of the spectra is listed along the left margin. The flux-calibrated profiles are shifted in the vertical direction for clarity in the figure, but no scaling has been applied. The location of the Mg II lines is indicated by the tick marks. The discontinuous lines mark the positions of $V_{hel} = -37, +12, +160$ km s^{-1}. The broad absorption component at SMC velocities seems to be variable and hence may contain contributions from stellar photospheric absorption features. The sharp component at $+160$ km s^{-1} remains fixed in four of the six spectra.

the predictions given in Smeding & Pottasch (1979), we obtain an estimate of the electron density for the $+312$ km s^{-1} region of $n_e \sim 100$ cm^{-3}.

We can use the column density derived for Si III of $\log[N(\mathrm{Si})/(1\ \mathrm{cm}^{-2})] \sim 13.00$ to 13.45, combined with a value of $\log[N(\mathrm{Si})/N(\mathrm{H})] = -5.63$ for the ISM of the SMC gaseous phase (Relaño & Peimbert 2001), to estimate the column density of $N(\mathrm{H}) \sim (4.3\text{–}12.0) \times 10^{18}$ cm^{-2} for the SNR shell. Adopting the electron density $n_e \sim 100$ cm^{-3} obtained above allows us to estimate the thickness of this shell to be $\sim(4.3\text{–}12.0) \times 10^{16}$ cm. Assuming that the SNR is relatively symmetric and adopting its diameter to be ~ 55 pc (from the nonthermal radio source; Ye et al. 1991) yields a total volume for the SNR shell of $(3.7\text{–}10.0) \times 10^{57}$ cm^3. Assuming 100 atoms cm^{-3} for this region yields a total mass of $(0.7\text{–}2.0) \times 10^{36}$ g $= 370$ to 1000 $M_\odot$. Clearly, the SNR shell contains a large amount of swept-up ISM gas.

5. SUMMARY AND CONCLUSIONS

We have presented the results obtained from the measurement of the ISM lines in the high-resolution *HST* STIS spectra obtained of the highly variable W-R system HD 5980 in the Small Magellanic Cloud. The principal results are the following:

1. Absorption components at $V_{hel} = +312 \pm 3$, $+343 \pm 3$, approximately $+33$, and $+64$ km s^{-1} are associated with the SMC supernova remnant SNR 0057−7226, which lies in the foreground, between HD 5980 and the Galaxy. The component at $+312$ km s^{-1} had been previously detected by de Boer & Savage (1980) and associated with an SNR by Fitzpatrick & Savage (1983). The two components at $v < 80$ km s^{-1} are blended with the Galactic ISM components. If the approaching and receding portions of the SNR shell have symmetric velocities, then the systemic velocity of the SNR is $+188$ km s^{-1}, which is in good agreement with the velocities of a selection of early-type stars in NGC 346 and thus suggests that the progenitor of this SNR was one of the most massive stars of this cluster, assuming coeval star formation. We obtain estimates of $T_e = 40{,}000$ K, $n_e = 100$ cm^{-3}, and $N(\mathrm{H}) \sim (4\text{–}12) \times 10^{18}$ cm^{-2} for the portion of the SNR shell that is responsible for the $+312$ km s^{-1} absorptions. A thickness for this shell of $\sim(4.3\text{–}12.0) \times 10^{16}$ cm is inferred. This implies a total mass of $(0.7\text{–}2.0) \times 10^{36}$ g $= 370$ to 1000 $M_\odot$ in the SNR.

2. Very high velocity narrow absorption components of Si IV λ1393 and λ1402 are detected at $V_{hel} = -1020, -840,$

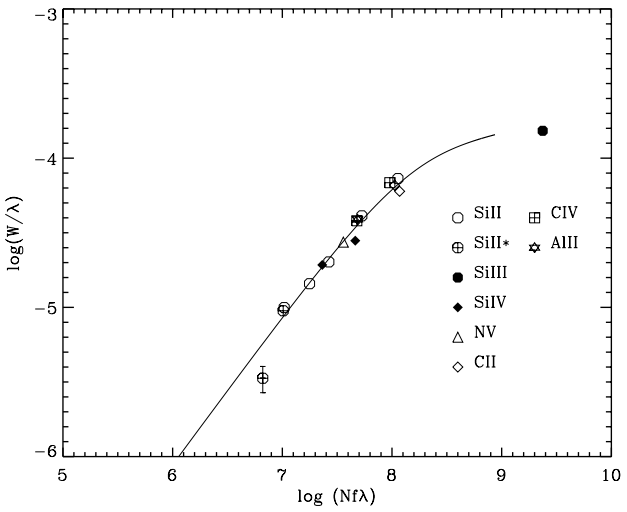

FIG. 10*a*

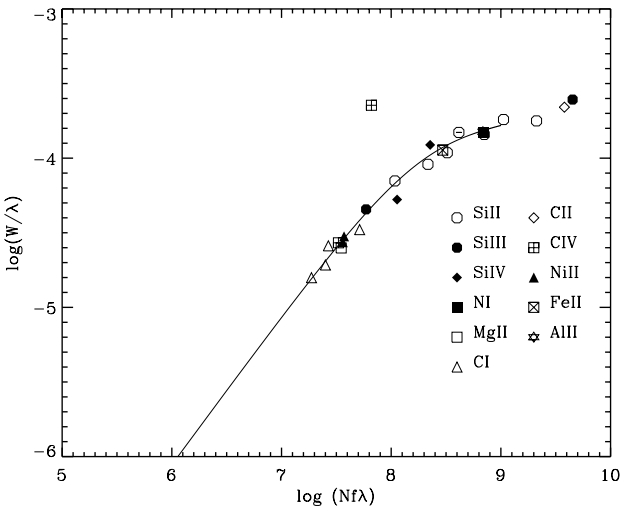

FIG. 10*b*

FIG. 10.—Curve of growth for (*a*) the $+312$ km s^{-1} SNR component and (*b*) the Galactic ISM components, obtained using the value $b = 10 \pm 2$ km s^{-1}

TABLE 6

COMPARISON OF COLUMN DENSITIES OBTAINED WITH TWO METHODS

	USING EQ. (1)			CURVE OF GROWTH		
LINE	Gal.	+312	+343	Gal.	+312	+343
C I λ1277	13.37	...	...	13.40	...	...
C I λ1328	13.36	...	...	13.40	...	...
C I λ1560	13.24	...	...	13.40	...	...
C I λ1656	13.21	...	...	13.40	...	...
C II λ1334.....	14.16	13.60:	...	15.00	13.84	...
C II* λ1335	13.84	13.68	13.19	...	13.84	12.95
C IV λ1548	...	13.77	...	...	13.51	...
C IV λ1550	13.36	13.51	...	13.40	13.51	...
N I λ1199	14.02:	...	...	14.50	...	...
N V λ1242	...	13.18:	...	...	13.57	...
Mg II λ1239.....	15.93	...	...	15.70	...	...
Si II λ1193	>13.53	12.89	12.50	14.60	12.95	12.20
Si II λ1304	>13.94	12.77	12.26	14.60	12.95	12.20
Si II λ1526	>13.67	12.67	12.32	14.60	12.92	12.20
Si II* λ1194	...	11.71:	12.31::	...	11.95	11.30
Si III λ1206.....	13.14:	12.93:	12.57:	14.40	13.45	12.30
Si IV λ1393.....	13.05*	12.64	...	13.60	12.81	...
Si IV λ1402.....	13.22*	12.78	<11.35	13.60	12.81	12.20
S II λ1250	15.07	...	...	15.25	...	...
S II λ1253	14.88	...	...	15.25	...	...
S II λ1259	14.77	...	...	15.25	...	...
S III λ1190	14.29	...	...	14.40	...	...
Fe II λ1608.....	14.11	12.69	12.85	14.60	...	...
Ni II λ1317.....	13.21	...	...	13.60	...	...

-630, -530, and -300 km s^{-1}, the strongest of which (at -530 km s^{-1}) has been reported previously (Koenigsberger et al. 2000). Several of these features are also present in S III λ1190.2, Si II λ1190.4, and C IV λ1550. The components at -1020 km s^{-1} (about -1170 km s^{-1} with respect to the SMC reference frame) are broader than the rest and are most likely discrete absorption components (DACs) generally associated with the winds of hot stars (Prinja & Howarth 1986). The other components all have FWHM $\sim$ 20–30 km s^{-1} and are likely to be associated with the circumstellar regions in which the fast stellar winds emitted after the 1994 eruption are interacting with the slow winds emitted during the 1993 and 1994 eruptive events. Although constant in velocity over the five *HST* observations obtained in 1999, there is a clear variation in these features between 1999 and 2000 consisting in a shift and/or doubling of the feature to higher velocities. These velocity changes correlate with the increase in the velocity of the DACs, possibly suggesting an association of these features. The interacting winds region now being observed in HD 5980 may constitute the earliest stage in the formation process of a windblown H II bubble ever observed.

3. The dominant velocities that we derive for the ISM components in the SMC are $V_{\rm hel} = +87 \pm 6$, $+110 \pm 6$, $+132 \pm 6$, $+158 \pm 8$, and $+203 \pm 15$ km s^{-1}. These velocities coincide with the four main gas complexes in the SMC at $V_{\rm hel} = 114 \pm 6$, 134 ± 9, 167 ± 8, and 192 ± 8 km s^{-1} that have been identified from a survey of H I 21 cm emission (McGee & Newton 1981, 1982). We estimate column densities for C I, C II, C IV, N I, N V, O I, Mg II, Si II, Si III, Si IV, P II, S II, Fe II, and Ni II for these velocity systems. The integrated column densities from the C I lines in the SMC yield $\log N({\rm C\ I}) = 13.01 \pm 0.04$, with the principal contribution arising in the 158 km s^{-1} system. We obtain a lower limit of the N I column density $\log N({\rm N\ I}) > 14.5$, with a more prominent contribution arising in the 132 and 158 km s^{-1} systems than in the 87 km s^{-1} system. A lower limit for O I is derived from the strong 1302 Å blend, $\log N({\rm O\ I}) > 15.70$, while the very weak line of O I λ1355 suggests $\log N({\rm O\ I}) \sim 16.9$ in the $+200$ km s^{-1} velocity system.

4. We obtain velocities and estimate column densities of ISM components at velocities assumed to arise in Galactic material. However, some of these suffer from probable contamination from the SNR's approaching shell.

5. From five of the six spectra, we obtain an upper limit for N V absorption at $V_{\rm hel} = 13 \pm 15$ km s^{-1} of 7 ± 3 mÅ, yielding an upper limit for the N V Galactic column density of $\log({\rm N\ V}) = 12.8^{+0.2}_{-0.3}$. The ISM component of this line at SMC velocities appears to be contaminated by stellar photospheric absorption.

G. K. thanks B. Savage, and Y.-H. Chu for helpful discussions, and the Centro de Ciencias Físicas, UNAM, where a large portion of this paper was written. We thank Daniel Pérez Becker for providing measurements of the stars in NGC 346, and A. Díaz, G. Zavala, L. Hernández and C. Guzman for their highly efficient support of the computing systems. Support for this work was provided by NASA through grants GO-7480.01-96A, GO-7480.02-96A, and GO-7480.03-96A from the Space Telescope Science Institute; from CONACYT grant 27744-E, and UNAM/DGAPA grant IN 113999. R. B. thanks Fundación Antorchas for providing support for this work.

REFERENCES

Baliunas, S. L., & Butler, S. E. 1980, ApJ, 235, L45
Chu, Y.-H., & Kennicutt, R. C., Jr. 1988, AJ, 95, 1111
Czyzak, S. J., & Aller, L. H. 1977, Ap&SS, 46, 371
de Boer, K. S., & Savage, B. D. 1980, ApJ, 238, 86
Fitzpatrick, E. L., & Savage, B. D. 1983, ApJ, 267, 93F
Frank, A., Balick, B., & Davidson, K. 1995, ApJ, 441, L77
García-Segura, G., Mac Low, M.-M., & Langer, N. 1996, A&A, 305, 229
Inoue, H., Koyama, K., & Tanaka, Y. 1983, in IAU Symp. 101, Supernova Remnants and Their X-Ray Emission, ed. J. Danziger & P. Gorenstein (Dordrecht: Reidel), 535
Humphreys, R. M., & Davidson, K. 1979, ApJ, 232, 409
Kelly, R. L., & Palumbo, L. J. 1973, Atomic and Ionic Emission Lines below 2000 Å (NRL Rep. 7599) (Washington: Nav. Res. Lab.)
Koenigsberger, G., Auer, L. H., Georgiev, L., & Guinan, E. 1998a, ApJ, 496, 934
Koenigsberger, G., Georgiev, L., Barbá, R., Tsvetanov, Z., Walborn, N. R., Niemela, V. S., Morrell, N., & Schulte-Ladbeck, R. 2000, ApJ, 542, 428
Koenigsberger, G., Peña, M., Schmutz, W., & Ayala, S. 1998b, ApJ, 499, 889
Koenigsberger, G., Shore, S., Guinan, E., & Auer, L. 1996, in Workshop on Colliding Winds in Binary Stars to Honor Jorge Sahade, ed. V. Niemela & N. Morell (Rev. Mexicana Astron. Astrofis. Ser. Conf. 5) (México D.F.: Inst. Astron., Univ. Nac. Autónoma México), 92
Massey, P., Parker, J. W., & Garmany, C. D. 1989, AJ, 98, 1305
McGee, R. X., & Newton, L. M. 1981, Proc. Astron. Soc. Australia, 4, 189
———. 1982, Proc. Astron. Soc. Australia, 4, 308
Moffat, A. F. J., et al. 1998, ApJ, 497, 896
Morse, J. A., Humphreys, R. M., & Damineli, A., eds. 1999, ASP Conf. Ser. 179, Eta Carinae at the Millennium (San Francisco: ASP)
Morton, D. C. 1991, ApJS, 77, 119
Niemela, V. S., Barbá, R. H., Morrell, N. I., & Corti, M. 1997, in ASP Conf. Ser. 120, Luminous Blue Variables, ed. A. Nota & H. J. G. L. M. Lamers (San Francisco: ASP), 222
Prinja, R. K., & Howarth, I. D. 1986, ApJS, 61, 357
Relaño, M., & Peimbert, M. 2001, in preparation
Savage, B. D., & de Boer, K. S. 1981, ApJ, 243, 460
Savage, B. D., Sembach, K. R., & Lu, L. 1997, AJ, 113, 2158
Schweickhardt, J., & Schmutz, W. 1999, in IAU Symp. 193, Wolf-Rayet Phenomena in Massive Stars and Starburst Galaxies, ed. K. A. van der Hucht, G. Koenigsberger, & P. R. J. Eenens (San Francisco: ASP), 101
Smeding, A. G., & Pottasch, S. R. 1979, A&AS, 35, 257
Songaila, A., Blades, J. C., Hu, E. M., & Cowie, L. L. 1986, ApJ, 303, 198
Spitzer, L. 1978, Physical Processes in the Interstellar Medium (New York: Wiley)
Staveley-Smith, L., Sault, R. J., Hatzidimitriou, D., Kesteven, M. J., & McConnell, D. 1997, MNRAS, 289, 225
Walborn, N. R. 1978, ApJ, 224, L133
Welty, D. E., Lauroesch, J. T., Blades, J. C., Hobbs, L. M., & York, D. G. 1997, ApJ, 489, 672
Woodgate, B. E., et al. 1998, PASP, 110, 1183
Ye, T., Turtle, A. J., & Kennicutt, R. C., Jr. 1991, MNRAS, 249, 722